-RESEARCH PAPER-

International Journal of Mining and Geo-Engineering

IJMGE

IJMGE 57-4 (2023) 427-434

DOI: 10.22059/ijmge.2023.364057.595093

Exploring Geothermal Potential through Multi-Modal Geophysical Data Integration: Gravity, Magnetic, and Magnetotelluric Prospecting

Ahmad Afshar [a,*], Gholam-Hossain Norouzi [b], Ali Moradzadeh [b]

[a] *Faculty of Mining Engineering, Amirkabir University of Technology, Tehran, Iran.*

[b] *School of Mining Engineering, College of Engineering, University of Tehran, Tehran, Iran.*

Article History:

Received: 19 August 2023.

Revised: 30 August 2023.

Accepted: 10 September 2023.

ABSTRACT

This study presents a comprehensive geophysical investigation of the Sabalan geothermal area in Iran, utilizing magnetic, gravity, and magnetotelluric (MT) data. These data have been inverted to a depth of 5000 meters. Magnetic data inversion accurately identified faults or fractures. Gravity data inversion produced a density model distinguishing intrusive masses, reservoirs, and cover units. MT data inversion utilized apparent resistivity and phase data for both TM and TE modes. The resulting models were compared with geological cross-sections to assess their accuracy and consistency. The integration of geophysical models yielded a comprehensive geological conceptual model for the Sabalan region. Heat sources, hydrothermal reservoirs, and potential geothermal fluid pathways were identified, demonstrating the effectiveness of geophysical methods in subsurface mapping. Consistency with newer Sabalan models based on drilling and geological data increased confidence in findings.

Keywords: *Geothermal exploration, Magnetic, Gravity, Magnetotelluric data inversion, Integrated interpretation, Sabalan area.*

1. Introduction

Geothermal resources stand as one of the most environmentally friendly renewable energy sources, presenting a feasible alternative to fossil fuels and hydrocarbons. Geothermal studies, aimed at quantifying the thermal characteristics of various geological areas worldwide, have been carried out by many researchers to explore highly potential geothermal reservoirs. The utilization of geothermal sources holds significant importance and is experiencing remarkable growth [1, 2].

The application of geophysical methods in geothermal resource exploration has gained substantial traction owing to their remarkable capabilities for subsurface analysis and imaging [3-5]. Geophysical techniques, including electrical surveys, electromagnetics, seismic method, gravity measurements, and magnetic surveys, have proven to be versatile and efficient tools for identifying and characterizing geothermal reservoirs. These methods provide invaluable insights by capturing diverse physical properties that are quantifiable through their respective approaches. Notably, variations in electrical resistivity and magnetic susceptibility within geothermal settings give rise to discernible anomalies, serving as key indicators of potential geothermal sources [6].

The integration of different geophysical methods allows for broader coverage and comprehensive analysis of subsurface structures. The amalgamation of geophysical data with geographic and geological information progressively assumes a pivotal role in visualizing and defining geothermal resources [7].

Geophysical research in the Sabalan region in northwestern Iran has played a significant role in the exploration of thermal resources. Focusing on the analysis of magnetic and gravity data, researchers have been able to investigate the deep-seated characteristics of the Earth, resulting in the determination of the Curie Point depth, geothermal gradient, and heat-flow estimations [5]. These geophysical studies have also contributed to identifying thermal anomalies and geothermal concentrations in the area. Ghaedrahmati, et al., (2013) conducted a 3-D inversion of magnetotelluric data from the Sabalan geothermal field, contributing to a deeper understanding of subsurface characteristics in the Sabalan area [8].

In this paper, an endeavor has been undertaken to formulate a novel conceptual model for the Sabalan region by employing the inversion of magnetic, gravity, and magnetotelluric (MT) data. By amalgamating the outcomes of these inversions, a conceptual model has been constructed, showcasing a notable level of congruence compared to the conceptual model derived from drilling results within the area.

2. Geothermal systems

2.1. Conceptual model

There are various types of geothermal resources, but generally, a geothermal system consists of a heat source, permeable rocks, and water surrounded by impermeable rocks (Fig.1). When water comes into contact with the hot rocks, the heated water or steam becomes trapped in permeable rocks and fractures beneath an impermeable layer of rock, creating a reservoir or geothermal source. Although this heated water can manifest itself as hot springs or geysers on the Earth's surface, it often remains confined deep within the Earth, within fractures and porous rocks. This collection of naturally heated water is referred to as a geothermal reservoir [6].

* Corresponding author. *E-mail address:* a.afshar@aut.ac.ir (A. Afshar).

Geothermal resources are categorized into different types based on their temperature and origin. These systems are classified into magmatic and non-magmatic systems, depending on whether they are related to magma emplacement or not. The magmatic type often encompasses hydrothermal systems (consisting of water or steam) with a flow regime, dry rock systems, and partial melting systems, while non-magmatic resources are frequently associated with hot fluids infiltrating sedimentary or crystalline environments [1].

Hydrothermal systems represent the most prevalent type of geothermal reservoirs, occupying a central role in scientific investigations concerning hydrothermal ones. These systems encompass a heat source, subsurface water for heat transportation and storage, along with encircling impermeable cap rocks. Geothermal fluids, acting as electrolytes, carry dissolved salts through the rock matrix. The temperature-dependent conductivity of both the fluid and the rock matrix results in reduced volume resistivity with rising temperatures. The enclosing cap rock of these reservoirs often responds to hydrothermal fluids spanning temperatures from just below 100 to beyond 200 degrees Celsius. This interaction gives rise to alteration zones within sedimentary layers, with the nature of alteration varying in response to temperature fluctuations [6, 9].

At lower temperatures (70 to 150 degrees Celsius), the cap rock is known as illite-smectite. However, at higher temperatures (180 degrees Celsius), minerals such as illite and chlorite are found within the interlayers of smectite. Around temperatures of 220 to 240 degrees Celsius, alteration is primarily dominated by minerals like chlorite and epidote. The alteration minerals at lower temperatures (illite-smectite) exhibit significantly lower specific electrical resistivity compared to the alteration minerals at higher temperatures (chlorite-epidote). Therefore, an increase in specific resistivity near the near-surface conductive layers (sedimentary cap rock) indicates a rise in temperature with depth, which is a characteristic indicator of high-temperature geothermal systems [10].

In a hydrothermal system, it is possible to illustrate the geothermal system using a conceptual model resembling Fig. 1-a. In a broader context, the upflow and outflow areas of a geothermal system cause the displacement of low-resistivity anomalies. The upflow region constitutes a portion of the reservoir where fluid predominantly ascends, leading to an increase in temperature with depth. Within this zone, the resistivity of the enveloping sedimentary cap rock progressively rises with depth due to heightened temperatures resulting from the presence of high-temperature minerals. In the cooler outflow regions, fluid movement is primarily horizontal, resulting in decreasing temperatures with depth (up to beneath the outflow zone). The low-resistivity anomaly of the sedimentary cap rock continues to extend toward shallower depths, causing the geometry of the conductive region to shift and become asymmetric in relation to the center of the geothermal reservoir (Fig. 1-b) [6].

Geothermal resources of non-magmatic origin exhibit a wide variety of geometries that make it challenging to present a unified conceptual model for them. Electrical resistivity anomalies in such types of resources originate from diverse sources and are often associated with the electrolytic conductivity of saline fluids. These fluids contain a significant number of dissolved salts, resulting in their electrical conductivity increasing with temperature. Consequently, in non-magmatic systems, imaging electrical resistivity is frequently employed to identify deep-seated groundwater reservoirs that are perceived as storage locations and pathways for geothermal flow[1].

2.2. Geophysical exploration of geothermal systems

The characteristic feature of active geothermal systems is the presence of a reservoir containing hydrothermal fluids at high temperatures, often causing alteration of the surrounding rocks. Hydrothermal alteration leads to changes in physical properties (such as electrical resistivity, density, magnetic susceptibility, and seismic wave velocity) of the medium. These anomalies can be detected using various geophysical methods, including geoelectric and electromagnetics, gravity, magnetic, and seismic techniques. Among these, electromagnetic methods, particularly magnetotellurics due to their significant penetration depth, play a crucial role in imaging the geometry of geothermal resources [4].

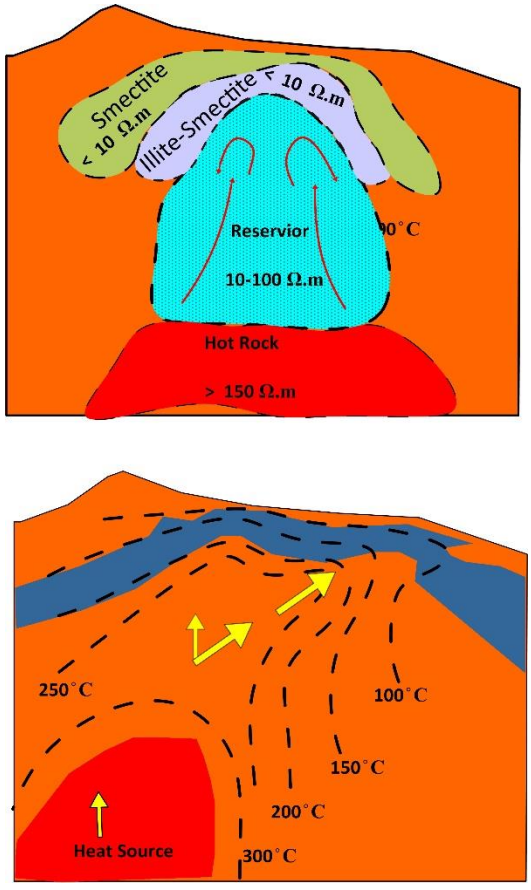

Fig. 1. Conceptual model of a hydrothermal geothermal source (a) in which alteratin zones exhibit lower specific resistivity compared to the enclosing rocks. A generalized conceptual model of the geothermal system is influenced by the geometry of upflow and outflow regions, causing resistivity anomalies not to be directly above the central storage area (b).

Geothermal systems often exhibit decreased electrical resistivity compared to the surrounding host rocks, which display resistivity anomalies. Furthermore, disparities in magnetic susceptibility and density are observed between geothermal reservoirs and cover units versus host rocks, often leading to noticeable negative anomalies. Volcanic formations like basalt, andesite, dacite, and rhyolite are indicative of geothermal systems due to their high presence of magnetic-susceptible minerals, such as magnetite, ilmenite, and titanomagnetite. As a consequence of hydrothermal alteration, these minerals can transform into secondary counterparts like pyrite, hematite, sphene, and clay minerals, which typically possess lower magnetic susceptibility than the primary minerals[4, 11].

In addition, depending on alteration intensity and other factors, other primary minerals (e.g., biotite, chromite, pyroxene, olivine) can undergo similar transformation into secondary minerals (e.g., feldspar, chlorite, clay minerals) with lower magnetic susceptibility. As a result, a diminished magnetic self-potential anomaly within a geothermal homogeneous rock unit, known for its higher self-potential, could indicate a zone of alteration[11].

In conclusion, variations in electrical resistivity, magnetic susceptibility, and density, along with the metamorphosis of magnetic minerals, offer valuable insights into the presence of geothermal systems. These distinct mineral characteristics and their altered forms can effectively guide geophysical investigations, aiding in the identification and delineation of hydrothermally altered zones and

potential geothermal reservoirs.

In geothermal systems, a distinctive hallmark is the presence of a reservoir containing hydrothermal fluids at elevated temperatures, often inducing alterations in the surrounding rock formations. These hydrothermal modifications give rise to shifts in the physical properties of the medium, encompassing attributes like electrical resistivity, density, magnetic susceptibility, and seismic wave velocity. The identification of these deviations can be accomplished through a range of geophysical techniques, encompassing geoelectric and electromagnetic methods, gravity, magnetic surveys, and seismic analyses. Within this toolkit, electromagnetic methodologies, particularly magnetotellurics recognized for their substantial penetration capabilities, assume a pivotal role in illuminating the structural intricacies of geothermal resources [3, 12].

On the other hand, hydrothermal fluids ascend to the Earth's surface through faults, fractures, and openings, reacting with the surrounding rocks. As a result, magnetic and gravity geophysical methods can also prove valuable in exploring geothermal resources by identifying the location of these faults and geological structures. Furthermore, magnetic methods, especially airborne magnetic data, are widely used for estimating the depth of the Curie point and exploring geothermal anomalies at a regional scale.

3. Geological Setting

The geothermal area of Sabalan is situated in the Ardabil province and the northwestern part of Mount Sabalan. Due to the presence of multiple hot springs in this region, a wide range of geophysical methods has been extensively employed throughout history for the exploration and modelling of geothermal sources. In summary, Sabalan represents a high-temperature magmatic geothermal system, located within the rocks of the Urumieh-Dokhtar magmatic belt within the tectonic framework of the continental margin [13].

Mount Sabalan comprises late Miocene to Quaternary trachyandesite, trachyte, and dacite volcanic rocks. The magmatic activity of the mountain can be divided into two stages: in the first stage, a substantial volume of ignimbrites and volcanic ashes erupted, interlayered with trachyandesite and trachytic andesite. Following several explosive phases, the primary destruction structure and the volcanic caldera ("caldera") were formed. In the second stage, dacitic to trachytic dacite domes were formed in the central section [14].

In Fig. 2, the geological map of the Sabalan region is presented. Generally, this area comprises glacial deposits, Quaternary sediments, trachyandesite flows (post-caldera with Pliocene age), trachytic to dacitic domes (concurrent with caldera formation), tuffs, and trachyandesite flows (pre-caldera). Based on exploration well data from NWS1 to NWS10 (Fig. 2), a geological cross-section (Section AB) has been prepared (Fig. 3). In summary, the stratigraphy of the area, from top to bottom, includes four main formations: Dezou Formation (Recent deposits), Valahzir Formation (including andesite, porphyritic dacite), Eocene andesite and trachyandesites (marked as "Ep" and "Epa" on the 100,000-scale Meshgin Shahr map), and intrusive rocks of the Azarini Suite (crystalline diorites and altered diorites containing secondary calcite, epidote, actinolite, and chlorite) [15, 16].

Tectonically, the dominant structural features of the region are strike-slip fault systems with a northwest-southeast trend, north-south normal faults, and northeast-southwest thrust faults.

4. Material and methodology

4.1. Inversion of potential filed data

For the inversion of potential field data, it suffices to invert a physical property as the objective function to minimize, as described in [17, 18]:

$$\varphi(m) = \varphi_d(m) + \beta\varphi_m(m) \quad (1)$$

Where $\varphi_d(m)$ represents the misfit function, β is the regularization parameter, and $\varphi_m(m)$ denotes the norm of the model. The misfit function is formulated as follows:

$$\varphi_d = \|W_d(Gm - d^{obs})\|^2 \quad (2)$$

In this equation, d^{obs} represents the vector of observed data (gravity or magnetic), G is the forward operator matrix with dimensions $N \times M$, m is the parameter vector of the model (density or magnetic susceptibility of cells), W_d is the data weighting matrix represented as a diagonal matrix $W_d = diag[1/\sigma_1 \ldots . 1/\sigma_n]$, where σ_i corresponds to the standard deviation (uncertainty) associated with the ith data. Here, φ_d is a variable with a chi-squared ($\chi^2{}_N$) distribution with N degrees of freedom, thus determining the misfit objective $\varphi_d{}^* \approx N$ for inversion leads to a solvable or acceptable solution for inversion [19].

For forward modelling of gravity and magnetic data, or in other words, to compute the forward operator matrix G, one can utilize the formulations provided by Rao et al. in 1990 and 1991 [20, 21]. The discrete representation of Equation 1 is expressed as follows:

$$\varphi_m(m) = (m - m_0)^T W_m{}^T W_m (m - m_0) = \|W_m(m - m_0)\|^2 \quad (3)$$

Where,

$$W_m{}^T W_m = \alpha_s W_s{}^T W_s + \alpha_x W_x{}^T W_x + \alpha_y W_y{}^T W_y + \alpha_z W_z{}^T W_z \quad (4)$$

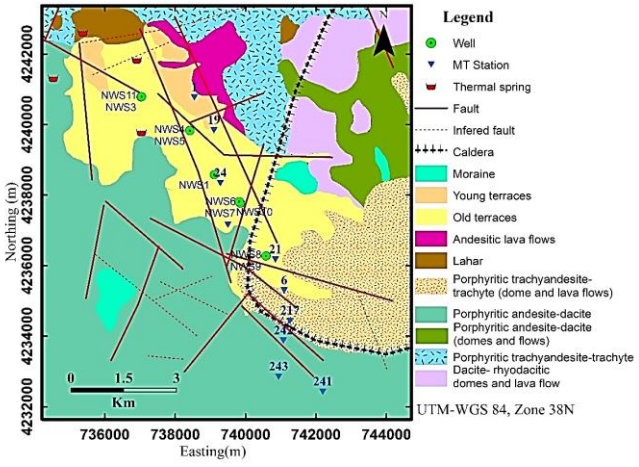

Fig. 2. Geological map of the Sabalan region with exploration well, magnetotelluric station, and modeling profile locations. Dashed line indicates approximate position of geological section AB (Fig. 3) based on exploration data.

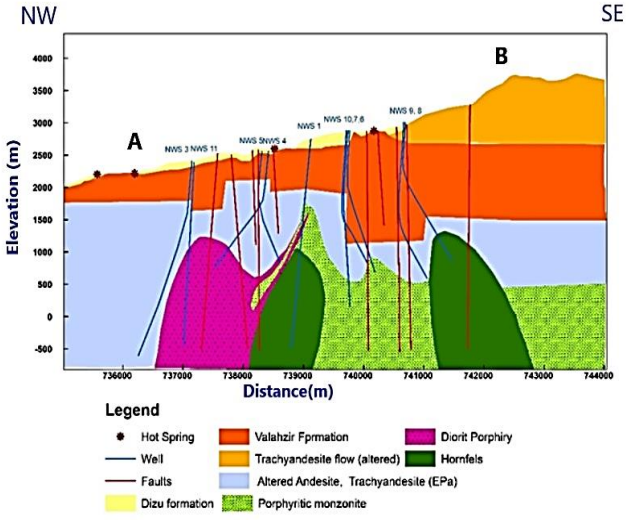

Fig. 3 Geological cross-section of section AB prepared based on exploration data from NWS1 to NWS11 (Fig. 2).

Here, W_s is a diagonal weighting matrix with its elements incorporates the depth weighting function and controlling the smoothness in horizontal and vertical directions. W_x, W_y, and W_z are adjusted based on the cell dimensions. α_s regulates the closeness of the derived model to the initial model, while α_x, α_y, and α_z control the roughness of the model in their respective directions[22].

The equation 3 is minimized by taking its derivative and setting it equal to zero.

$$\left(G^T {W_d}^T W_d G + \beta {W_m}^T W_m\right)m = G^T {W_d}^T W_d d^{obs} + \beta {W_m}^T W_m m_0 \quad (5)$$

The equation 5, which has a general form of Ax=b, can be solved using various methods. In this article, the dual-gradient method was employed to solve Equation 5.

4.2. Analysis and inversion of MT data

The most crucial step in the inversion of magnetotelluric data is the dimensional analysis and determination of the physical property distribution for exploratory purposes. In this paper, the phase tensor method has been employed for determination of geoelectrical dimension [23, 24].

4.2.1. Dimensional analysis

Caldwell (2004) introduced the phase tensor ($\emptyset$) parameter, which proves highly effectivein the dimensional analysis of magnetotelluric data[24]:

$$\emptyset = \begin{bmatrix} \emptyset_{xx} & \emptyset_{xy} \\ \emptyset_{yx} & \emptyset_{yy} \end{bmatrix} = X^{-1}Y \quad (6)$$

Where X is the real part and Y is the imaginary part of the impedance tensor ($Z = X + iY$). By decomposing the singular value, the dimensional analysis parameters of the phase tensor are obtained as follows:

$$\beta_p = 1/2\, tan^{-1}\left(\frac{\emptyset_{xy}-\emptyset_{yx}}{\emptyset_{xx}+\emptyset_{yy}}\right), \alpha_p = 1/2\, tan^{-1}\left(\frac{\emptyset_{xy}+\emptyset_{yx}}{\emptyset_{xx}-\emptyset_{yy}}\right) \quad (7)$$

In this context, β_p represents the skew angle and α_p stands for the ellipticity of the phase tensor. To visually depict the phase tensor, an ellipse is utilized, where $\alpha_p - \beta_p$ denotes the angle of the major axis extension of the ellipse. Its skewness matrix is zero for two-dimensional structures. For one-dimensional structures, the phase tensor appears as a circle, while for two-dimensional structures, the lengths of the major and minor axes of the ellipse differ, and $|\beta_p| \leq 3°$. Additionally, by plotting the azimuth angle of $\alpha_p - \beta_p$, the orientation of geoelectric anisotropy can be determined[23, 24].

4.2.2. Two-dimensional forward modelling of MT dat

To perform the forward modelling, The equations corresponding to TM and TE modes were substituted into Maxwell's equations to begin the process. This yields a set of differential equations. By numerically solving these equations using numerical methods, we can obtain the apparent resistivity, phase, and complex conductivity parameters for the desired frequencies. The differential equations for the E_x and H_x components are as follows[25, 26]:

$$\frac{\partial}{\partial y}\left(\frac{1}{i\omega\mu}\frac{\partial E_x}{\partial y}\right) + \frac{\partial}{\partial z}\left(\frac{1}{i\omega\mu}\frac{\partial E_x}{\partial z}\right) - (\sigma + i\omega\varepsilon)E_x = 0 \quad (8)$$

$$\frac{\partial}{\partial y}\left(\frac{1}{\xi+i\omega\varepsilon}\frac{\partial H_x}{\partial y}\right) + \frac{\partial}{\partial z}\left(\frac{1}{\xi+i\omega\varepsilon}\frac{\partial H_x}{\partial z}\right) - i\omega\mu H_x = 0 \quad (9)$$

Here, μ represents magnetic permeability, ε represents dielectric permittivity, and ξ represents electrical conductivity. The above equations are second-order differential equations that can be solved for each cell while considering appropriate boundary conditions. This process allows us to determine the values of E_x and H_x.

4.2.3. Two-Dimensional Magnetotelluric Inversion

The magnetotelluric inversion is commonly expressed as a numerical solution to the operator equation:

$$d = G(m) \quad (10)$$

Where d represents the data vector, m is the model vector, and G stands for the forward modelling function. However, it is important to note that the magnetotelluric inverse problem is characterized as ill-posed. Consequently, the results of the inversion are both unstable and nonunique. This indicates that various geological-electrical models can potentially match the observed data with similar accuracy [27].

In this study, the Occam inversion method was employed, and the key equations have been succinctly provided. To solve the operator equation (10), the general objective function is formulated as follows[27]:

$$min\ \|Lm\|_2\ ,\ subject{:}\ \|G(m) - d^{obs}\| \leq {\varphi_d}^* \quad (11)$$

Here, L represents the model roughness matrix, and ${\varphi_d}^*$ signifies the measure of misfit. It is assumed that noise or errors present in the data are independent and normally distributed. The fundamental idea of this method is iteratively applied through local linearization, utilizing Taylor's method for linearization[27]:

$$G(m^k + \Delta m) \approx G(m^k) + J(m^k)\Delta m \quad (12)$$

Where $\Delta m = m_{k+1} - m_k$ and J is the Jacobian matrix of G(m) with respect to the model parameters. The objective of the smooth inversion is to minimize the model roughness norm‖Lm‖. To achieve this, the objective function is expressed as a regularized least squares problem and incorporates a stabilization parameter β [28]:

$$\varphi(m,\beta) = \|Lm\|^2 + \beta^{-1}\left(\|W_d(G(m) - d^{obs})\|^2 - {\varphi_d}^{*2}\right) \quad (13)$$

By linearizing the objective function and subsequently setting its derivative to zero, an iterative solution for the problem is obtained:

$$m^{k+1} = m^k[\beta L^T L + [W_d J(m^k)]^T W_d J(m^k)]^{-1}[W_d J(m^k)]^T W_d \hat{d}_k \quad (14)$$

Where $\hat{d}_k = d^{obs} - G(m^k) + J(m^k)m^k$. This iterative approach aims to optimize the model parameters for a better fit to the observed data while considering the regularization term to ensure stability and uniqueness in the inverse solution[28].

The 2D finite element code developed by Wannamaker et al. (1987) was used for conducting the forward modelling. To compute the partial derivatives of G(m) with respect to conductivity, the adjoint method was employed as described in deLugao and Wannamaker (1996)[25, 29].

4.3. Geophysical dataset of the study area

4.3.1. Magnetic and gravity data

The magnetic data along the AB section (Fig. 2) were acquired with a station spacing of 50 meters using the GEM-19T magnetometer. For inversion, the area beneath the AB section was discretized into square cells of dimensions 200 meters. Considering the profile length of 9200 meters, the modelling was extended to a depth of 5000 meters. Fig. 4 displays the inversion results of the magnetic data using the mentioned method.

Gravity data within the study area were collected along the AB profile at 200-meter intervals using a Scintrex Cg3 gravimeter. After necessary corrections and removal of regional effeect, the residual gravity data were inverted. In Fig. 5a, the observed residual gravity anomalies are displayed and the calculated anomalies are presented for comparison. The cross-section resulting from gravity modelling is illustrated in Fig. 5b.

4.3.2. Magnetutelluric Data

In pursuit of geothermal potential, EDC (2008, 2010) executed an MT survey within Iran's Sabalan geothermal area, deploying an irregular grid of 78 stations to gather data. This initiative aimed to identify favorable zones for geothermal development[8]. Time series data, encompassing two electric field components and three magnetic field components, were meticulously collected at both local and remote stations via the Phoenix MTU-5A data acquisition system. Subsequent to data acquisition, the Phoenix Geophysics, Ltd. SSMT2000 software

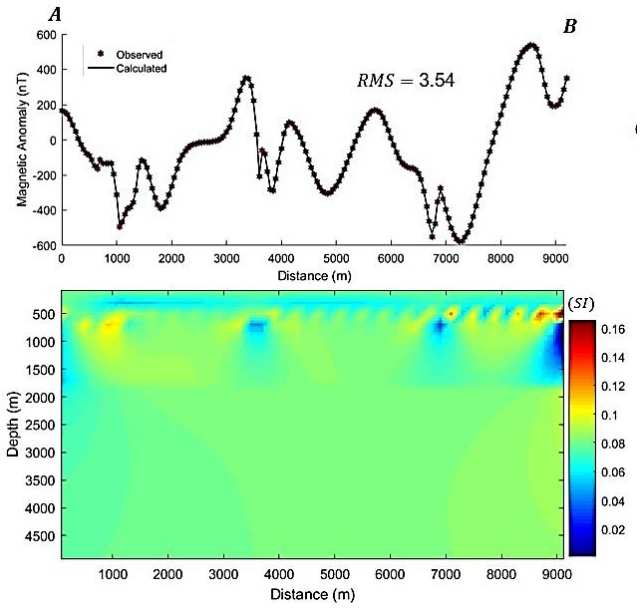

Fig. 4. The result of magnetic data inversion (section AB in Fig. 3) a) observed and calculated magnetic anomaly. b) Susceptibility model resultant from the inversion.

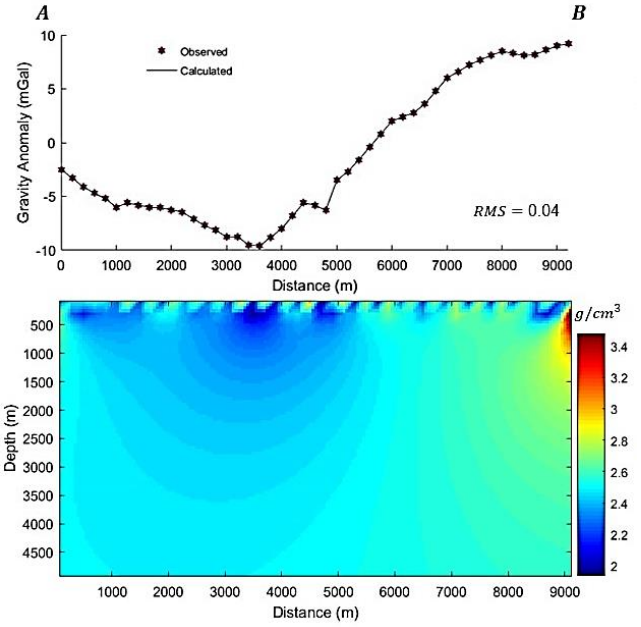

Fig.5. Inversion results of gravity data along cross-section AB. a) Observed and calculated curves of residual gravity anomaly. b) Density model obtained from 2D inversion.

was employed in the data processing stage to estimate the impedance tensor and tipper from the recorded time series data.

The data processing stage involved estimating the impedance tensor (comprising apparent resistivity and phase) across 68 periods spanning from 0.0031 to 357 seconds. From this dataset, we focused on 10 specific stations along profile AB. The chosen station locations have been visually depicted on the geological map of the study area, presented in Fig. 2.

Before performing the inversion of magnetotelluric data, a dimensional analysis was carried out using the phase tensor method. As illustrated in Fig. 6, within the frequency range of 0.1-100 Hz, the conditions for a two-dimensional structure ($|\beta| \leq 3°$) predominantly hold true. At higher frequencies (shallower depths), the predominant strike of the geoelectric structure is nearly northward (with the major axis of the impedance tensor ellipse aligned in the trigonometric direction of the x-axis). However, with decreasing frequency (increasing depth), the main structure becomes northeast-southwest oriented. Despite the 90-degree ambiguity, the rose diagram of the α-β angle distribution supports this observation. Consequently, it can be inferred that the deep geoelectric structure beneath the region is roughly oriented in the N35E direction, which is nearly perpendicular to the selected profile. For this reason, prior to modelling, the impedance tensor data have been rotated to align with this orientation.

For the 2D inversion of MT data, a modelling approach similar to the potential field data (Fig. 4b and 5b) is employed. The region beneath the AB section is discretized into 200-meter grid cells, reaching depths of up to 5000 meters. The 2D inversion utilizes both apparent resistivity and phase data for both TM and TE modes in the frequency range of 0.1 to 100 Hz (Fig. 7a-7d).

As mentioned, the Occam's method was employed for the inversion, and the values of RMS and model norm for 33 iterations are depicted in Fig. 8. It is observed that the RMS value has stabilized approximately from the 26th iteration onwards. Hence, the apparent resistivity model obtained from this iteration is considered the final result of the inversion (Fig. 9). In Fig.7e-7h, pseudo-sections of apparent resistivity and phase for both TM and TE modes are presented for the calculated data resulting from modelling. The RMS value for the entire dataset is obtained to be 1.4.

4.4. Evaluation of the results with geological information and conceptual model

In order to interpret and assess the inversion results, as well as to compare them with the geological cross-section AB (Fig. 3), a contour representation of the models resulting from the inversion of AB section data has been prepared in Fig. 10.

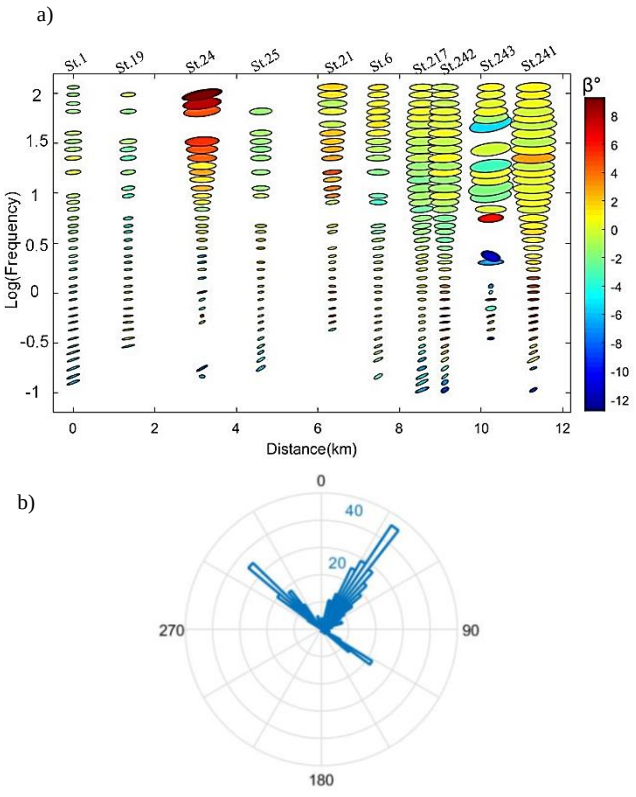

Fig. 6. MT Station Phase Tensor of AB Profile (a) and α-β Angle Rosette Diagram (b). Black Triangles: MT Station Locations.

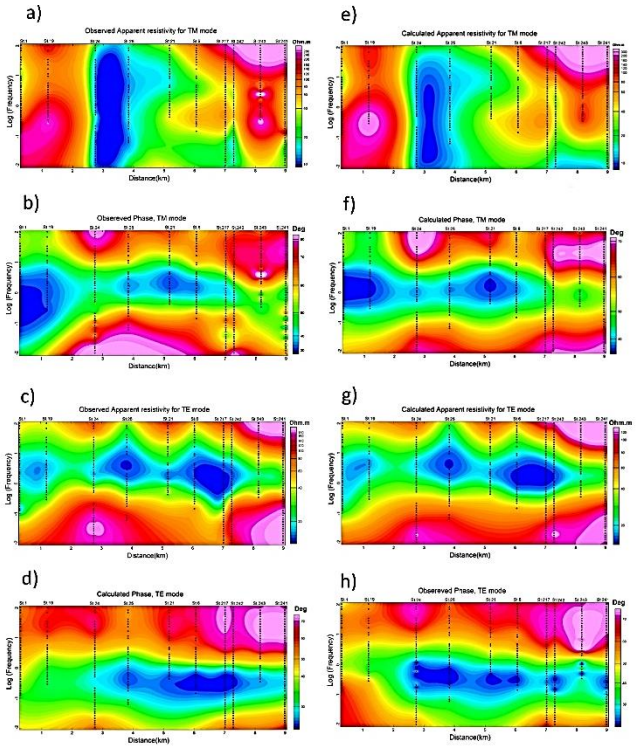

Fig. 7: Pseudo-Sections of Apparent Resistivity mode (a) and Phase (b) for TM Mode, Pseudo-Sections of Apparent Resistivity (c) and Phase (d) for TE Mode Inversion of AB Profile after Impedance Tensor Rotation to N35E Orientation. e-h) Pseudo-Sections of Calculated Apparent Resistivity and Phase for Both TM and TE Modes Obtained from Occam's Inversion of Data these data.

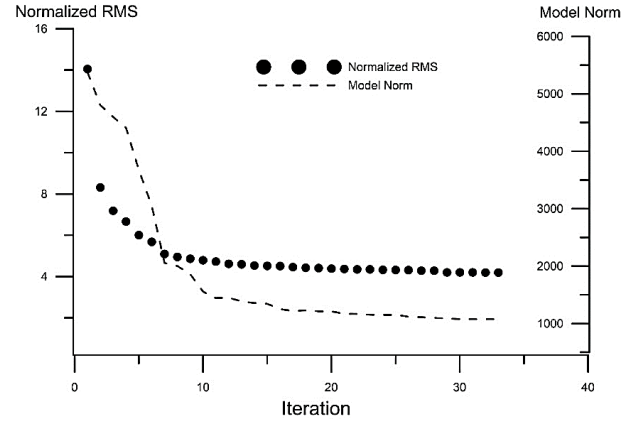

Fig. 8. Normalized RMS Error and Model Norm in 33 Iterations of Occam's Method for Magnetotelluric Data Inversion of AB Profile.

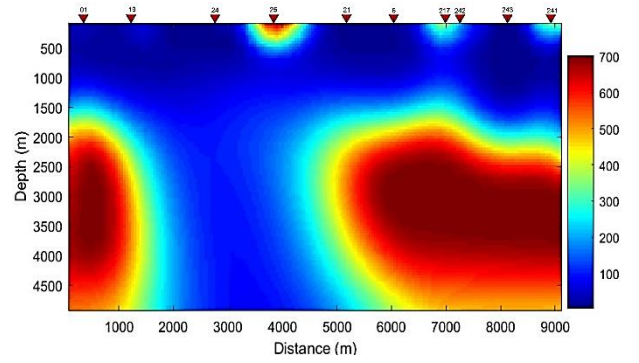

Fig. 9. Apparent Resistivity Model Obtained from Inversion of Magnetotelluric Data of AB Profile.

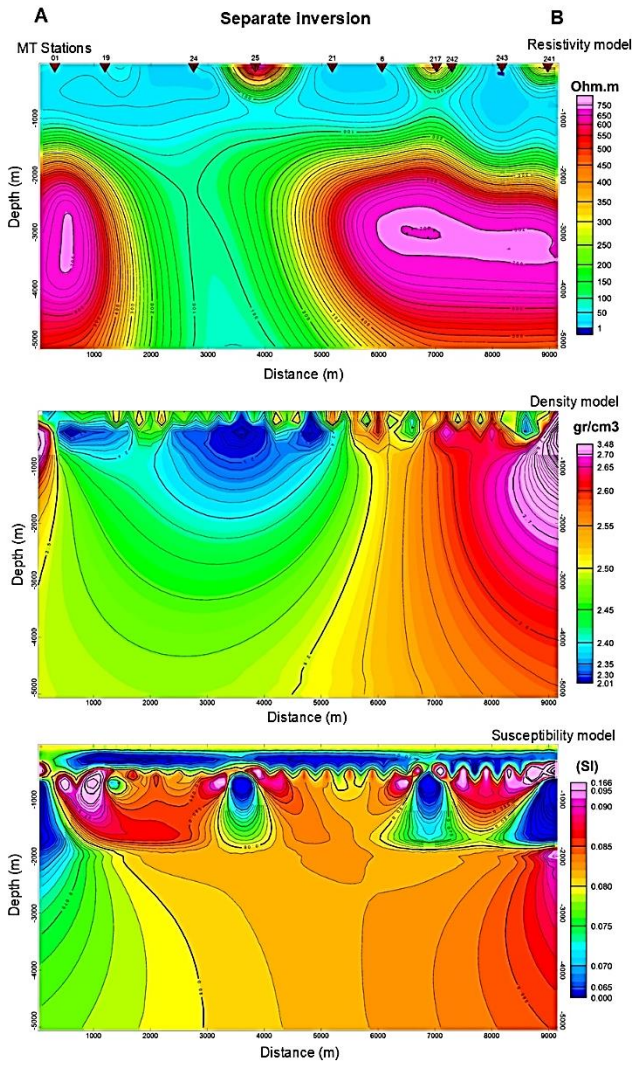

Fig. 10. Contour Representation of Inversion Results for Magnetotelluric (a), Gravity (b), and Magnetic (c) Data.

As observed in Fig.10a, the model resulting from the inversion of MT data demonstrates a good overall representation of the geological structure when compared to the geological cross-section. However, possibly due to the scarcity of high-frequency data or the influence of near-surface disturbances, and the relatively large station spacing in the initial portion of the profile, the resolving power is reduced. The density model obtained from gravity data inversion, although generally distinguishing the intrusive mass, reservoir, and clay cover units up to a depth of 5000 meters, exhibits lower resolution for shallower depths (Fig. 10b).

Regarding the magnetic susceptibility model, a plausible distinction emerges, allowing the identification of hydrothermal alterations, typically characterized by lower susceptibilities (less than 0.07), within the background. This distinction aligns well with inferred faulting patterns (illustrated by the dashed black line in Fig. 10c), displaying a remarkable correspondence with fault positions in the geological cross-section. However, the magnetic model exhibits less satisfactory performance for depths exceeding approximately 2000 meters. This behavior may be attributed to the inherent characteristics of the magnetic field, which experiences more pronounced attenuation with increasing depth in comparison to the gravity data.

By comparing the density and magnetic susceptibility models with the geological cross-section (Fig. 3), it can be inferred that regions of high magnetic susceptibility and density anomalies within the initial segment of the profile might correspond to a dioritic intrusive body.

Furthermore, the prominent anomaly at the end of the profile, characterized by increased intensity, could be attributed to the upwelling of a thermal intrusion, consistent with the conceptual model of a heat source. The apparent resistivity model corroborates these findings and additionally suggests the low-resistivity deviation (less than 50 ohm-meters) towards the beginning of the profile, indicating the potential pathways for geothermal fluid migration.

By integrating the inversion-derived models, a comprehensive geological conceptual model for the AB profile has been developed (Fig. 11). This model exhibits a high level of consistency with the latest Sablan conceptual model [30], which is prepared based on geological information and boreholes.

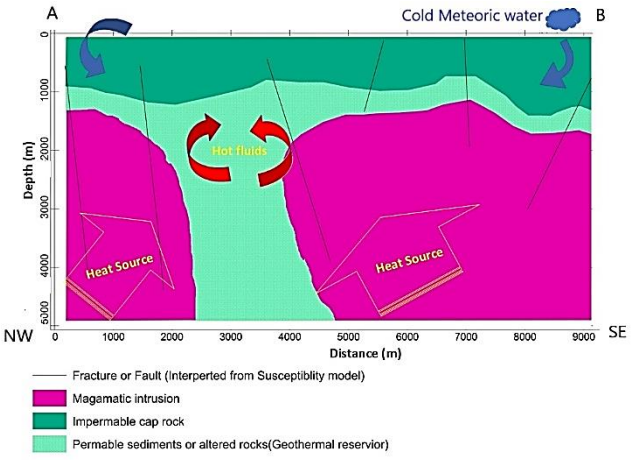

Fig. 11. Conceptual Geothermal Model of the Sabalan Area Resulting from the Integration of Inversion Results for Magnetotelluric, Magnetic, and Gravity Data.

5. Discussion

Based on the findings of this study, it is recommended to conduct further research in the field of joint inversion of gravity, magnetic, and magnetotelluric data to enhance the accuracy and resolution of subsurface structures. Additionally, developing predictive geological conceptual models by integrating geophysical and geological data for other regions with similar geothermal potential could contribute to an improved identification of heat sources. To enhance the accuracy and resolution in identifying subsurface structures, the utilization of intelligent data fusion methods like fuzzy clustering for combining multi-type data such as gravity, magnetic, and magnetotelluric data can be explored. Additionally, employing joint inversion methods for multi-source geophysical data can contribute significantly to improved and more accurate interpretation and assessment of subsurface characteristics in geothermal regions.

6. Conclusion

In this study, a comprehensive geophysical approach was employed to investigate the subsurface characteristics of the Sabalan geothermal area in Iran. Magnetic and gravity data were collected along a profile, yielding valuable insights into the geological structures. Magnetotelluric (MT) data were also utilized to examine the deep geoelectric properties of the region. Through MT data inversion, resistivity model was generated, providing significant deep subsurface information.

The integration of these geophysical models enabled the development of a comprehensive geological conceptual model for the Sabalan region. By comparing the models with the geological cross-section, we identified heat sources, hydrothermal reservoir, and potential pathways for geothermal fluid flow. Our results demonstrated the effectiveness of the employed geophysical methods in delineating subsurface structures and identifying geothermal areas.

Furthermore, the consistency of our estimated models with the newer Sabalan model, based on drilling and geological data, increases our confidence in the accuracy of the findings. The combination of geophysical and geological information has provided us with a deeper understanding of the geological features and geothermal potential of the Sabalan area.

This study underscores the importance of geophysical investigations in mapping subsurface structures and assessing thermal potentials. The developed geological conceptual model offers valuable insights for further research and development activities in the Sabalan geothermal region. Our findings contribute to a broader understanding of the region's geology and its potential for resource exploitation.

Acknowledgments

The authors extend their heartfelt gratitude to the Department of Mining and Metallurgical Engineering at the Amirkabir University of Technology, as well as the School of Mining Engineering at the University of Tehran, for their generous support and resources that greatly contributed to the successful completion of this research. We would also like to express our appreciation to the respected editor and anonymous reviewers for their valuable contributions and feedback.

REFERENCES

[1]. Munoz, G., Exploring for geothermal resources with electromagnetic methods. Surveys in geophysics, 2014. 35(1): p. 101-122.

[2]. Dashti, A. and M. Gholami Korzani, Study of geothermal energy potential as a green source of energy with a look at energy consumption in Iran. Geothermal Energy, 2021. 9(1): p. 28.

[3]. Pearson-Grant, S., P. Franz, and J. Clearwater, Gravity measurements as a calibration tool for geothermal reservoir modelling. Geothermics, 2018. 73: p. 146-157.

[4]. Lichoro, C.M., K. Árnason, and W. Cumming, Resistivity imaging of geothermal resources in northern Kenya rift by joint 1D inversion of MT and TEM data. Geothermics, 2017. 68: p. 20-32.

[5]. Afshar, A., et al., Curie Point Depth, Geothermal Gradient and Heat-Flow Estimation and Geothermal Anomaly Exploration from Integrated Analysis of Aeromagnetic and Gravity Data on the Sabalan Area, NW Iran. Pure and Applied Geophysics, 2017. 174(3): p. 1133-1152.

[6]. Kana, J.D., et al., A review of geophysical methods for geothermal exploration. Renewable and Sustainable Energy Reviews, 2015. 44: p. 87-95.

[7]. Gallardo, L.A. and M.A. Meju, Structure-coupled multiphysics imaging in geophysical sciences. Reviews of Geophysics, 2011. 49(1): p. RG1003.

[8]. Ghaedrahmati, R., et al., 3-D inversion of MT data from the Sabalan geothermal field, Ardabil, Iran. Journal of Applied Geophysics, 2013. 93: p. 12-24.

[9]. Kong, Y., et al., Recent studies on hydrothermal systems in China: a review. 2014. 2: p. 1-12.

[10]. Ussher, G., et al. Understanding the resistivities observed in geothermal systems. in proceedings world geothermal congress. 2000.

[11]. Pandarinath, K., et al., Magnetic susceptibility of volcanic rocks in geothermal areas: application potential in geothermal exploration studies for identification of rocks and zones of hydrothermal alteration. Arabian Journal of Geosciences, 2014. 7(7): p. 2851-2860.

[12]. Mandal, A., et al., Integrated geophysical investigation to map shallow surface alteration/fracture zones of Atri and Tarabalo hot springs, Odisha, India. Geothermics, 2019. 77: p. 24-33.

[13]. Torbehbar, A.K. and M.H. Liseroudi. Geological Classification of Proposed Geothermal Areas of Iran. 2014.

[14]. Shahbazi Shiran, H., Petrogenesis of Quaternary Shoshonitic Volcanism in NE Iran (Ardabil): Implication for Postcollisional Magmatism. Journal of Geological Research, 2013. 2013: p. 11.

[15]. Amini, Meshkin Shahr Geological Map in Scale of 1/100000. 1998, GSI: Iran.

[16]. Bogie, I., K. Khosrawi, and B. Talebi, Geological results from the drilling of the Northwest Sabalan geothermal project, Iran. Proceedings, WGC, 2005.

[17]. Li, Y. and D.W. Oldenburg, 3-D inversion of magnetic data. Geophysics, 1996. 61(2): p. 394-408.

[18]. Li, Y. and D.W. Oldenburg, 3-D inversion of gravity data. Geophysics, 1998. 63(1): p. 109-119.

[19]. Cella, F. and M. Fedi, Inversion of potential field data using the structural index as weighting function rate decay. Geophysical Prospecting, 2012. 60(2): p. 313-336.

[20]. Rao, D.B., M. Prakash, and N.R. Babu, 3D AND 2½ D MODELLING OF GRAVITY ANOMALIES WITH VARIABLE DENSITY CONTRAST. Geophysical Prospecting, 1990. 38(4): p. 411-422.

[21]. Rao, D.B. and N.R. Babu, A rapid method for three-dimensional modeling of magnetic anomalies. Geophysics, 1991. 56(11): p. 1729-1737.

[22]. Oldenburg, D.W. and Y. Li, Inversion for applied geophysics: A tutorial. Near-surface geophysics: SEG, 2005: p. 89-150.

[23]. Booker, J.R., The magnetotelluric phase tensor: a critical review. Surveys in Geophysics, 2014. 35(1): p. 7-40.

[24]. Caldwell, T.G., H.M. Bibby, and C. Brown, The magnetotelluric phase tensor. Geophysical Journal International, 2004. 158(2): p. 457-469.

[25]. Wannamaker, P.E., J.A. Stodt, and L. Rijo, A stable finite element solution for two-dimensional magnetotelluric modelling. Geophysical Journal International, 1987. 88(1): p. 277-296.

[26]. Franke, A., R.-U. Börner, and K. Spitzer, Adaptive unstructured grid finite element simulation of two-dimensional magnetotelluric fields for arbitrary surface and seafloor topography. Geophysical Journal International, 2007. 171(1): p. 71-86.

[27]. Degroot-Hedlin, C. and S. Constable, Occam's inversion to generate smooth, two-dimensional models from magnetotelluric data. Geophysics, 1990. 55(12).

[28]. Constable, S.C., R.L. Parker, and C.G. Constable, Occam's inversion: A practical algorithm for generating smooth models from electromagnetic sounding data. Geophysics, 1987. 52(3): p. 289-300.

[29]. Aprea, C., J.R. Booker, and J.T. Smith, The forward problem of electromagnetic induction: accurate finite-difference approximations for two-dimensional discrete boundaries with arbitrary geometry. Geophysical Journal International, 1997. 129(1): p. 29-40.

[30]. Seyedrahimi-Niaraq, M., et al., Development of an updated geothermal reservoir conceptual model for NW Sabalan geothermal field, Iran. Geothermal Energy, 2017. 5(1): p. 14.